RSC Advances

RSC Publishing

PAPER

View Article Online
View Journal | View Issue

Cite this: *RSC Adv.*, 2013, **3**, 20024

The synergy effect on Li storage of $LiFePO_4$ with activated carbon modifications†

Bo Wang,[ab] Qiuming Wang,[a] Binghui Xu,[b] Tiefeng Liu,[a] Dianlong Wang*[a] and George Zhao*[b]

Received 8th July 2013
Accepted 14th August 2013

DOI: 10.1039/c3ra44218g

www.rsc.org/advances

In this work, composite electrodes containing lithium iron phosphate ($LiFePO_4$) and activated carbon (AC) were prepared by physically mixing $LiFePO_4$ and AC with polyvinylidene fluoride (PVDF) as a binder and acetylene black (AB) as an electrically conductive agent. X-ray diffraction (XRD), field-emission scanning electron microscopy (FESEM), high-resolution transmission electron microscopy (HRTEM), nitrogen sorption, four-probe conductivity and vibrating densitometer techniques were employed to characterize samples. The characterization results showed that the presence of AC increased the electrical conductivity, reduced the tap density, and modified the porosity of the resultant composite electrode materials. Electrochemical data demonstrated that the composite electrode displayed a significantly improved electrochemical performance in comparison with the pure $LiFePO_4$ electrode. An electrode with 5 wt% AC exhibited specific discharge capacities of 70 mA h g^{-1} at 20 C and 100 mA h g^{-1} at 10 C without significant capacity decay after 400 cycles. Galvanostatic charge–discharge and cyclic voltammetry results revealed that energy was stored *via* both charge adsorption and lithium intercalation/deintercalation owing to the presence of both AC and $LiFePO_4$ in the composite electrode. Electrochemical impedance spectroscopy (EIS) was used to investigate the charge–discharge kinetics and mechanism of the composite electrode. The EIS results demonstrated that the two different active materials ($LiFePO_4$ and AC) displayed synergy in terms of both material structure and energy storage, contributing to the observed excellent electrochemical performance.

Introduction

Lithium-ion batteries (LIBs) and electrochemical double-layer capacitors (EDLCs) are two important energy storage devices. The most striking feature of the former is their high specific energy density whereas that of the latter is their high specific power density.[1–7] The combination of the key features of these two energy storage systems can be realized by configuring hybrid electrochemical energy storage systems known as lithium-ion capacitors (LICs), which can be configured either in series or parallel.[8] The serial configuration consists of one EDLC electrode and one LIB electrode while the parallel configuration consists of LIB/EDLC composite electrodes as both electrodes.

For the serial LICs system, Amatucci and co-workers[9] were the first to demonstrate such a device using $Li_4Ti_5O_{12}$ as the anode and activated carbon (AC) as the cathode. The device showed an inspiring electrochemical performance at a high rate (10 C) with only about 10% capacity loss after 5000 cycles. Subsequent studies[10,11] using different LIB and EDLC materials confirmed the improvement of electrochemical performance.

Different from the serial configuration, the parallel LIC system can be achieved by utilizing composite electrodes consisting of both LIB and EDLC active materials with different energy storage mechanisms – faradaic reactions for the LIB active material and charge adsorption for the EDLC active material.[12] The parallel LICs have been reported to outperform both LIBs and EDLCs in terms of power and energy densities.[13] Recently, the improvement of electrochemical performances of a $LiMn_2O_4$/AC composite electrode was investigated by Cericola *et al.*[12] The results clearly showed that the presence of different types of material in a composite electrode benefited the electrode property, thus, effectively improving the electrochemical performances.

Olivine-type $LiFePO_4$ (LFP) is one of the most promising cathode materials for LIBs due to its high theoretical capacity, excellent cycling stability, low cost, environmental friendliness and improved safety.[14–24] AC, on the other hand, is the most commonly utilized material for EDLCs due to its low cost, high specific surface area, excellent cycle stability, and easy preparation.[25] Correspondingly, composite electrode materials

[a]*Harbin Institute of Technology, School of Chemical Engineering and Technology, Xidazhi Street, 150001 Harbin, China. E-mail: wangdianlongwbhit@163.com; Fax: +86 45186413721; Tel: +86 45186413751*

[b]*The University of Queensland, Faculty of Engineering, Architecture and Information Technology, School of Chemical Engineering, St Lucia, Brisbane, QLD 4072, Australia. E-mail: george.zhao@uq.edu.au; Fax: +61 7 33654199; Tel: +61 7 33469997*

† Electronic supplementary information (ESI) available. See DOI: 10.1039/c3ra44218g

consisting of LFP and AC have been studied for parallel LICs.[26–30] Hu *et al.*[26,27] reported a LFP/AC composite prepared using the solid-state reaction method. The composite was used as a composite cathode material in a LIC. An improved cycling performance and increased specific capacity were observed. However, they did not give further analysis for the above behaviours. Böckenfeld *et al.*[29,30] prepared LFP/AC composite electrodes with different ratios of LFP over AC. It was found that the specific capacities of the composite electrodes were higher than that of the sum of the specific capacities of the LFP and AC electrodes measured under the same experimental conditions. The authors also observed that the AC functioned similarly to other conductive carbon materials, such as carbon fibres and multi-walled carbon nanotubes, which enhance the electrical conductivity of the composite and prevent LFP particles from aggregation. Nevertheless, they only discussed the improvement performance from the structural perspective, while neglected the perspective of energy-storing.

In this work, the composite electrodes consisting of LFP and AC of different mass ratios were prepared by physically mixing of LFP and AC with acetylene black (AB) as conducting agent and polyvinylidene fluoride (PVDF) as binder. The electrochemical properties of the composite electrodes during charge–discharge processes were studied using electrochemical impedance spectroscopy (EIS) technique, which has proven to be a powerful tool for characterization of electrochemical systems.[31] Based on the results from both physical and electrochemical characterizations, we attempted to explain the mechanism of electrochemical improvement – the synergy between AC and LFP components from both structural and energy-storing perspectives.

Experimental

Preparation of the electrodes

The composite electrodes studied in this work were prepared by physically mixing electrochemically active materials LFP (space group of *Pnmb*, Likai Co. Ltd., Taiwan, more information about XRD can be seen from Fig. S1†) and AC (Kuraray Co. Ltd., Japan, specific surface area $S_{BET} = 1241.6\ m^3\ g^{-1}$, microporous volume $V_{micropores} = 0.40\ cm^{-3}\ g^{-1}$, mesoporous volume $V_{mesopores} = 0.31\ cm^{-3}\ g^{-1}$, macroporous volume $V_{macropores} = 0.044\ cm^{-3}\ g^{-1}$, total pore volume $V_{total\ pores} = 0.75\ cm^{-3}\ g^{-1}$, and tap-density $\rho = 0.35\ g\ cm^{-3}$, more information about BET can be seen from Fig. S2†) with 10 wt% acetylene black (AB) and 10 wt% polyvinylidene fluoride (PVDF) binder in *N*-methylpyrrolidone (NMP) solvent to form a slurry, which was then pasted on an Al foil and dried at 100 °C for 10 h in a vacuum oven. The composite electrodes prepared with different masses of AC are designated as *w*%LAC, where *w* stands for the weight percentage in the composite electrodes. For comparison purpose, electrodes containing pure LFP and AC respectively with the same amounts of both AB and PVDF in the same solvent were also prepared. All electrodes were cut into disks with a diameter of 1.4 cm, the average mass loading of which was about 2.2 mg cm^{-2}, and stored in an argon atmosphere in a glove box. The electrodes studied in this work are summarized in Table 1.

Characterizations

X-ray diffraction (XRD) patterns were collected from a D/max-γB X-ray diffractometer (Rigaku, Japan) using Cu Kα radiation ($\lambda = 1.54178$ Å). The diffraction angle ranged from 10° to 60° two theta with a scanning rate of $0.02°\ s^{-1}$. The morphology and microstructure of the active materials and electrodes were characterized by using field-emission scanning electron microscopy (FESEM, Hitachi, S-4800) and high-resolution transmission electron microscopy techniques (HRTEM, JEM-2100). Nitrogen sorption isotherms were measured using Micromeritics ASAP 2020 at 77.3 K. The electrical conductivities of the AB, AC, LFP and LAC were measured at room temperature using a four-probe conductivity test metre (SB120; San Feng). The tap-density of the powders was tested by adding a given amount of the powder to a dry measuring cylinder, which was subsequently tapped until the volume of the powder was no longer changed. The ratio of the mass and the volume of the powder gave the tap-density.

Electrochemical measurements

For electrochemical measurements, button cells (CR2025) were assembled with the above-prepared disks as the cathode, metallic lithium disks as the anode, polypropylene membrane (Celgard 2400) as the separator, and ethylene carbonate (EC)–dimethyl carbonate (DMC)–diethyl carbonate (DEC)-based (1 : 1 : 1 by weight) electrolyte with 1 M $LiPF_6$ dissolved in. For the LAC electrodes, both LFP and AC were considered as the active material so that the specific capacity was calculated on the basis of the total masses of LFP and AC in the composite electrodes.

The cells were charged and discharged over a voltage range of 2.5–4.2 V (*vs.* Li/Li^+) at different current rates, which were independent of the testing procedure, using a Battery Testing System (Neware, China). The charge–discharge rates are expressed as *n*C/*n*D, where *n*C/*n*D means the charge current is set up to achieve the theoretical charge–discharge capacity of the electrode in 1/*n* h. Here, we assume that the theoretical charge–discharge capacity of the active material in different electrodes is 170 mA h g^{-1} uniformly. For example, 10C–10D means to achieve the theoretical charge–discharge in 6 min with the charge–discharge density of 3.4 A g^{-1}. Electrochemical impedance spectroscopy (EIS) and cyclic voltammetry (CV) data were collected on an electrochemical workstation (PARSTAT 2273, Princeton Applied Research, USA). The CV measurement

Table 1 Formulas of the tested electrodes

Electrode	Active material	Conductive additives	Binder
3%LAC	3 wt% AC + 77 wt% LFP	10 wt% AB	10 wt% PVDF
5%LAC	5 wt% AC + 75 wt% LFP	10 wt% AB	10 wt% PVDF
10%LAC	10 wt% AC + 70 wt% LFP	10 wt% AB	10 wt% PVDF
15%LAC	15 wt% AC + 65 wt% LFP	10 wt% AB	10 wt% PVDF
LFP	80 wt% LFP	10 wt% AB	10 wt% PVDF
AC	80 wt% AC	10 wt% AB	10 wt% PVDF

was carried out at a scanning rate of 0.5 mV s^{-1} between 2.5 and 4.2 V. The EIS measurement was performed over a frequency range of 100 kHz to 10 mHz at different states of charge (SOCs) and discharge (SODs) with an applied amplitude of 5 mV. The parameters of the equivalent circuit were calculated and analyzed by computer simulations using the ZSimpWin software and the relative standard deviations were within 10%.

Results and discussion

Electrochemical performance

Fig. 1 compares the rate performance (discharge capacity) of different electrodes at charge–discharge rates ranging from 1C–1D to 20C–20D. It is seen that all composite electrodes exhibited a better electrochemical performance, especially at high rates, than the pure LFP electrode. Particularly, the 5%LAC electrode displayed the highest rate capacity (100 mA h g^{-1} at 10C–10D and 70 mA h g^{-1} at 20C–20D). At the same charge–discharge rates, the pure LFP electrode only delivered about 85 and 45 mA h g^{-1} respectively. On the other hand, the AC electrode showed a high capacity retention even at 20C–20D with a capacity of 26 mA h g^{-1}, which is about 70% of the capacity at 1C–1D (38 mA h g^{-1}). The high capacity retention of the AC electrode is not surprising because of its electric double layer energy storage mechanism. However, it should be noted that the rate performance of the AC electrode, particularly at high rates, might be limited by the kinetics of the lithiation/delithilation of the anode (metallic lithium disk), which was used as the counter electrode.[32] The above results confirmed that AC is an appropriate active component for making composite cathodes for LICs. However, the amount of AC added in the composite electrodes should be controlled due to its low specific capacity (38 mA h g^{-1} at 1C–1D and 26 mA h g^{-1} at 20C–20D) and low tap density (0.35 g cm^{-3} for AC and 1.32 g cm^{-3} for LFP).

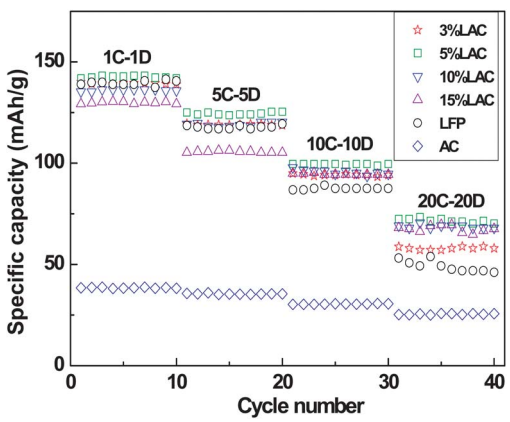

Fig. 1 Rate performance (discharge capacity) of different electrodes.

The observed improvement on rate performance can be understood by comparing the specific capacity obtained experimentally, C_e, with that predicted by using linear combination of each component in the composite electrode, C_p, which is given in eqn (1) as suggested by Fernando[33] and Böckenfeld:[29]

$$C_p = (f_{LFP} \times C_{LFP} + f_{AC} \times C_{AC}) \quad (1)$$

where C_{LFP} and C_{AC} are the capacities delivered by LFP and AC, respectively, and f_{LFP} and f_{AC} are the mass fractions of the two active materials, which can be calculated from eqn (2):

$$f_x = m_x/(m_{LFP} + m_{AC}) \quad (2)$$

The difference between C_e and C_p, ΔC, is then given by:

$$\Delta C = C_e - C_p \quad (3)$$

The values of C_e, C_p and ΔC at different rates are presented in Table 2. ΔC is of great use to investigate the improvement of composite electrodes if any favorable synergy takes place between the components in the composite. $\Delta C = 0$ indicates no synergy, $\Delta C > 0$ indicates a favorable synergy, which can be quantified as an additional capacity. It clearly can be seen, ΔC increases with the increase in current rate, which implies that the synergy becomes more and more intense. What's more, when the contents of AC $\geq$ 5 wt%, the values of ΔC in different composite electrodes are similar at the same current rates and 5%LAC electrode has largest capacities, which indicates that a small addition of AC can effectively build the synergy while too much will lower the capacity.

To investigate the synergy between AC and LFP, sample 5% LAC with the best rate performance was chosen for further study. The charge–discharge profiles of LFP and 5%LAC at current rates of 5C–5D are shown in Fig. 2a. 5%LAC exhibited an improved specific capacity of 121 mA h g^{-1} in comparison with 100 mA h g^{-1} of LFP. It is seen that the voltage plateau of 5%LAC was lengthier than that of LFP with a decreased polarization between the charge and discharge plateaus from 0.63 to 0.30 V, indicating that the electron transportation kinetics in electrode 5%LAC was improved by the addition of AC (the electric conductivities of AC, LFP and 5%LAC are

Table 2 C_e, C_p and ΔC at each rate of different electrodes

	AC/mA h g^{-1}	LFP/mA h g^{-1}	3%LAC/mA h g^{-1}			5%LAC/mA h g^{-1}			10%LAC/mA h g^{-1}			15%LAC/mA h g^{-1}		
Parameters	C_{AC}	C_{LFP}	C_e	C_p	ΔC	C_e	C_p	ΔC	C_e	C_p	ΔC	C_e	C_p	ΔC
1C–1D	38	140	139	136	3	142	134	8	136	127	9	130	121	9
5C–5D	35	117	119	114	5	124	112	11	120	107	13	114	102	12
10C–10D	31	88	94	86	8	100	84	16	97	81	16	95	77	18
20C–20D	26	46	57	45	12	72	45	27	69	44	25	68	42	26

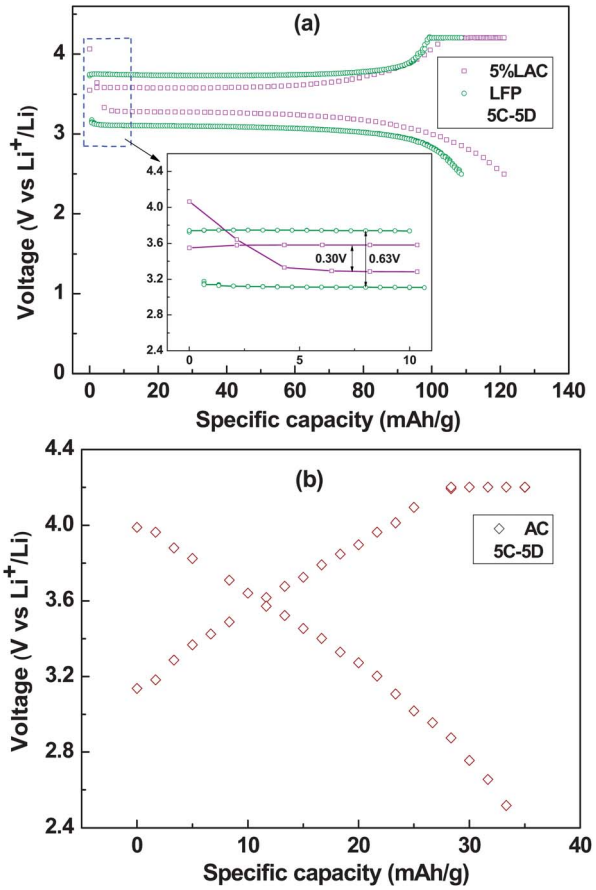

Fig. 2 Charge–discharge profiles of (a) 5%LAC and LFP, and (b) pure AC.

4.62×10^{-3} S cm^{-1}, 1.56×10^{-8} S cm^{-1} and 6.28×10^{-6} S cm^{-1}, respectively). It also can be seen from the enlarged profiles in the capacity range of 0–10 mA h g^{-1} (inset of Fig. 2a) at the beginning of discharge that the voltage descends rapidly from the highest cutoff potential (4.2 V) to the plateaus potential (3.3 V), which is probably due to the presence of AC in the composite electrode. From the charge–discharge profiles of pure AC electrode measured under the same experimental conditions shown in Fig. 2b, a typical capacitive charge–discharge profiles with potential continuously ascends/descends between the lowest cutoff potential (2.5 V) and the highest cutoff potential (4.2 V) is indeed seen. The AC electrode had a capacity of about 35 mA h g^{-1} (72 F g^{-1}), however, there was only 5 wt% of AC in 5%LAC electrode, which would contribute only about 1.7 mA h g^{-1} (3.6 F g^{-1}) to the overall electrode capacity, this is much lower than the difference between 5%LAC and LFP (about 10 mA h g^{-1}). Therefore, it is believed that the electrochemical performance of the composite electrodes cannot be a simply combined of the contributions of the two electrode materials, AC and LFP. There could be a synergy between the two components as has been observed previously.[24,26–30] Interestingly, the capacitive charge profile at the beginning of charge for electrode 5%LAC was not obvious, showing the asymmetry between the charge process and the discharge process of the composite electrodes.

The charge current and capacity (efficiency) as a function of time of electrodes LFP and 5%LAC at 20C–1D are shown in Fig. 3. As can be seen, LFP electrode did not show any galvanostatic charge process, which was due to overlarge polarization.[24] While for the 5%LAC electrode, the time of the galvanostatic charge process (followed by a constant-voltage process) was approximately 100 s and the charge capacity during this process was around 90 mA h g^{-1}, which is nearly 65% of the total charge capacity (142 mA h g^{-1}). Moreover, after charging for 160 s, the charge efficiency of electrode 5%LAC was about 80%, much higher than that of electrode LFP (only 50%). These results indicate an excellent fast-charge characteristic of the LAC composite electrode.

The high-rate cycling performance at 10C–10D of electrodes LFP and 5%LAC is shown in Fig. 4. It is clearly seen that LFP delivered a discharge capacity of about 55 mA h g^{-1} after 400 cycles, which is only about 65% of its initial capacity. On contrast, electrode 5%LAC showed a significantly improved cycling stability with a discharge capacity of around 100 mA h g^{-1} during the 400th cycle, which is approximate 100% of the initial discharge capacity.

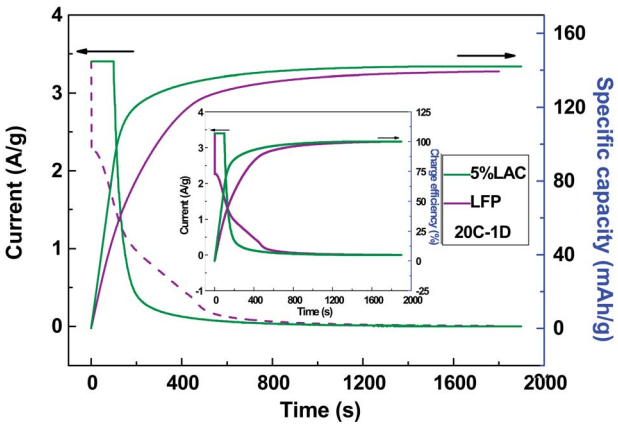

Fig. 3 The charge current and capacity (efficiency) as a function of time for fast-charging performance.

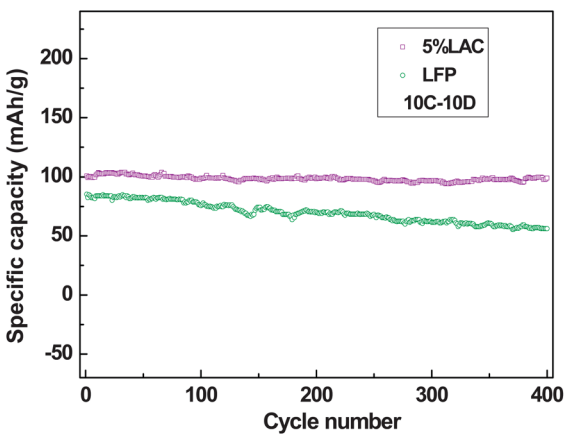

Fig. 4 High-rate cycling performances at 10C–10D of 5%LAC and LFP.

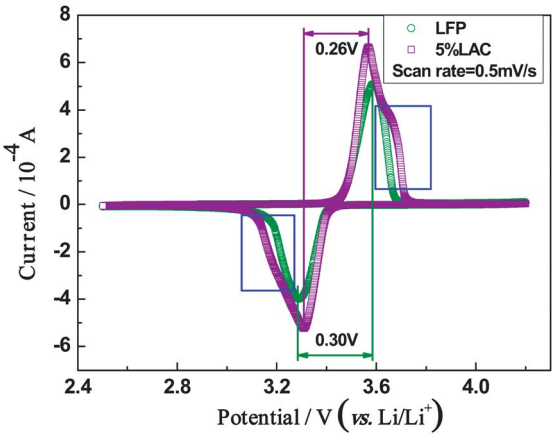

Fig. 5 Cyclic voltammetry profiles of LFP and 5%LAC.

CV and EIS testing

The CV plots of electrodes LFP and 5%LAC are shown in Fig. 5. In comparison with LFP, electrode 5%LAC exhibited sharper anodic/cathodic peaks, larger peak currents, and smaller separation between the anodic/cathodic peaks (0.26 V of 5%LAC *vs.* 0.30 V of LFP), suggesting a better electrochemical performance of 5%LAC.[34] In addition, electrode 5%LAC showed a higher response current than electrode LFP in the voltage range as highlighted by the blue box. It is evident that such a response current of electric double layer originated from the AC component in 5%LAC. The results suggest that the LFP in the composite electrode appeared to be more electrochemically active, which was probably induced by AC.

Along with CV, EIS technique was employed to study the electrochemical properties of electrode LFP and composite electrode 5%LAC, contrastively. Symmetric Li–Li cells were investigated to examine the contribution of the Li/electrolyte interface to the impedance. Due to the existence of two identical interfaces in the symmetric cell, the interfacial resistance of one single interface was considered half of the resistance observed from the data.[35,36]

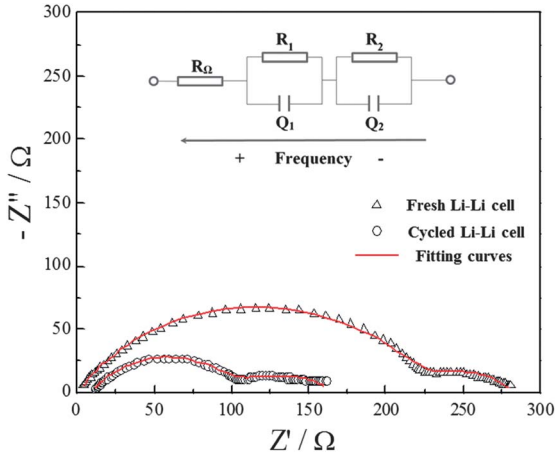

Fig. 6 The impedance spectra of a Li–Li cell before cycling and after 400 cycles.

The impedance spectra of a fresh Li–Li symmetric cell together with a Li–Li symmetric cell fabricated with Li electrodes after being charged–discharged for 400 times in a LFP–Li cell at 10C–10D are shown in Fig. 6. The equivalent circuit, as shown in the inset of Fig. 6, is proposed to fit the impedance spectra of Li–Li cell. R_Ω refers to the ohmic resistance including the resistance of the electrolyte, electrode leads and terminals. The resistance–capacitance ($R//C$) circuit unit usually used to signify the semicircles in the impedance spectra, here, constant phase element Q is employed instead of an ideal capacitor C in order to take into account the non-ideal frequency response of the displayed data. Y_0 (Ω^{-1} s^n) and n are used to depict constant phase element Q.[37] The Q represents a resistor when "n" $\sim$ 0, a capacitor when "n" $\sim$ 1, an inductor when "n" $\sim$ -1, and a Warburg resistance when "n" $\sim$ 0.5.[38] $R_1//Q_1$ are corresponding to the passivation layer on the Li metal surface (the high-frequency arc seen from Fig. 6), and $R_2//Q_2$ are relating to the charge-transfer process on Li metal surface (the low-frequency arc seen from Fig. 6).

The fitting curves and parameters of the components fitted by ZSimpWin software using the $R_\Omega(R_1//Q_1)(R_2//Q_2)$ model are presented in Fig. 6 by solid line and Table 3, respectively. The excellent fitting curves indicate significantly decreased R_1 (227.4 Ω of the fresh cell *vs.* 88.9 Ω of the cycled cell), which is attributed to the dendrites grown at the metallic Li surface.[39] It is seen from Table 3 that the R_2 values measured using the fresh and cycled cells were almost the same (53.37 Ω of the fresh cell *vs.* 63.26 Ω of the cycled cell).[35,36]

The impedance spectra of a LFP–Li cell and a 5%LAC–Li cell during the 400th cycle are shown in Fig. 7, where x represents the content of Li in one unit cell of LFP. Due to the symmetry and asymmetry between the charge process and discharge process of LFP electrode and 5%LAC electrode, as is seen from Fig. 2, only different SOCs were examined for LFP–Li cell and both different SOCs and SODs were examined for 5%LAC–Li cell.

The equivalent circuit, as shown in the inset of Fig. 7a, is proposed to fit the impedance spectra of LFP–Li cell with R_Ω as the ohmic resistance, $R_1//Q_1$ corresponding to the charge transfer process on the interface of LFP/electrolyte in the high-frequency region, $R_2//Q_2$ relating to the charge transfer process on the interface of Li/electrolyte in the mid-high-frequency region and Q_0 corresponding to the ion diffusive behavior in the low-frequency region.[40,41] The information of passivation layer on the Li metal surface is not considered here, due to the

Table 3 Circuit parameters for the Li–Li cell

Parameters	R_Ω/Ω	R_1/Ω	$Q_1 - n$	$Q_1 - Y_0/\Omega^{-1}$ s^n	R_2/Ω	$Q_2 - n$	$Q_2 - Y_0/\Omega^{-1}$ s^n
Fresh cell	0.9242	227.4	0.6784	1.7×10^{-5}	53.37	0.618	0.0074
Cycled cell	9.949	88.9	0.6798	3.1×10^{-5}	63.26	0.623	0.0076

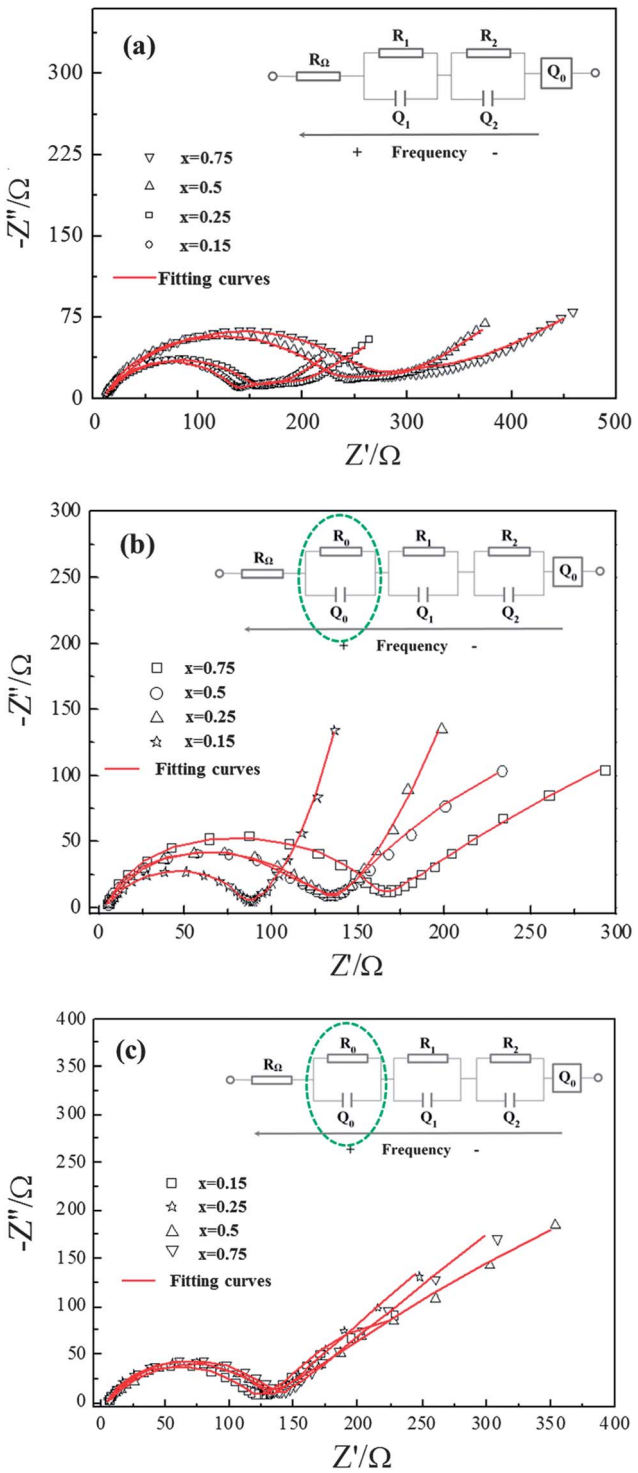

Fig. 7 The impedance spectra of a LFP–Li cell at different SOCs (a) and a 5%LAC–Li cell at different SOCs (b) and SODs (c) during the 400th cycle.

approximate time constant about this electrochemical process with that of the charge-transfer process of LFP/electrolyte interface.[42] For the equivalent circuits of 5%LAC–Li cell, as shown in the insets of Fig. 7b and c, one more $R_0//Q_0$ parallel elements is added in the high frequency region to describe the resistance and capacitance of the surface and pores of AC.[43,44]

Table 4 Circuit parameters for the LFP–Li cell

	Different SOCs			
Parameters	$x = 0.75$	$x = 0.5$	$x = 0.25$	$x = 0.15$
R_Ω/Ω	6.384	4.693	4.735	5.417
R_1/Ω	245.09	212.87	146.46	123.33
$Q_1 - n$	0.7491	0.7911	0.7339	0.817
$Q_1 - Y_0/\Omega^{-1}\ s^n$	7.57×10^{-6}	6.22×10^{-6}	1.16×10^{-6}	1.47×10^{-6}
R_2/Ω	38.89	33.23	12.49	21.31
$Q_2 - n$	0.5859	0.5714	0.8238	0.6463
$Q_2 - Y_0/\Omega^{-1}\ s^n$	2.86×10^{-3}	2.57×10^{-3}	2.37×10^{-3}	4.41×10^{-3}
$Q_0 - n$	0.4341	0.5	0.4439	0.5193
$Q_0 - Y_0/\Omega^{-1}\ s^n$	0.01468	0.01926	0.0222	0.0353

The fitting curves are presented as the solid lines in Fig. 7b and c and the parameters of the components fitted by ZSimpWin software using the $R_\Omega(R_1//Q_1)(R_2//Q_2)Q_0$ model for LFP–Li cell and the $R_\Omega(R_0//Q_0)(R_1//Q_1)(R_2//Q_2)Q_0$ model for 5%LAC–Li cell are presented in Tables 4 and 5, respectively.

It can be seen from Fig. 7 that each plot consisted of a quasi-semicircle in the high-frequency region, followed by a line in the low-frequency region and all the semicircles became weaker and weaker with the decrease of x in Li_xFePO_4.[45,46] Fig. S3† compares R_1 of electrodes LFP and 5%LAC at different SOCs from the values listed in Tables 4 and 5. It is clearly seen that each R_1 of 5%LAC–Li cell is smaller than that of LFP–Li cell at the same SOC, indicating a lower resistance for charge transfer as result of improved electric conductivity of 5%LAC. In addition, with decrease of x in Li_xFePO_4, R_1 of both LFP–Li cell and 5%LAC–Li cell are smaller and smaller, revealing the decrease of charge transfer resistance. One reason applied to explain this phenomenon is that the ionic conductivity of the cathode materials increases with the proceeding of charge.[45,46]

It is worth noting that there is an obvious difference between the lines in the low-frequency region of the charge and discharge processes of 5%LAC–Li cell as shown in Fig. 7b and c. The slope of the lines during the charging process became higher and higher with the decrease of the value of x in Li_xFePO_4, indicating a capacitive behavior in the charge process.[47,48] However, this behavior was not obvious in discharge process. It is also can be seen from Table 5 that the values of "n" for Q_0 of charge process increase with the proceeding of charge and at the end of this process, the values are close to 1 indicating a capacitive property. As to discharge process, the "n" of Q_0 are similar with values of about 0.5 suggesting a Warburg resistance.[38]

The differences between the absorption and desorption processes for anionic groups (PF_6^{-1}) absorbing to or desorbing from the surface and pores of AC can be used to explain both the differences of impedance spectra in the low-frequency (Fig. 7) region and charge–discharge profiles (Fig. 2).[13,26,27] The nitrogen adsorption/desorption isotherms and pore-size distributions of AC, LFP and 5%LAC samples are shown in Fig. S2.† The pores in AC used in this work are mainly microporous and a part of mesoporous (~4 nm) pores with microporous volume $V_{micropores} = 0.40\ cm^{-3}\ g^{-1}$ and mesoporous volume $V_{mesopores} = 0.31\ cm^{-3}\ g^{-1}$, respectively. 5%LAC showed a similar pore sizes

Table 5 Circuit parameters for the 5%LAC–Li cell

	Different SOCs				Different SODs			
Parameters	$x = 0.75$	$x = 0.5$	$x = 0.25$	$x = 0.15$	$x = 0.15$	$x = 0.25$	$x = 0.5$	$x = 0.75$
R_Ω/Ω	4.492	4.446	5.186	4.11	5.099	4.655	5.185	5.499
R_0/Ω	15.17	87.08	27.848	6	15.35	9.16	25.42	36.491
$Q_0 - n$	0.917	0.9264	0.8813	0.9631	0.9006	0.894	0.918	0.9723
$Q_0 - Y_0/\Omega^{-1}\ s^n$	0.2227	0.2384	1.8×10^{-5}	1.2×10^{-5}	0.2242	0.114	2.4×10^{-5}	5.9×10^{-5}
R_1/Ω	112.1	103.53	84.7	51.24	112.3	98.75	80.4	59.9
$Q_1 - n$	0.859	0.8066	0.7904	0.8259	0.7586	0.7926	0.8159	0.7893
$Q_1 - Y_0/\Omega^{-1}\ s^n$	8.2×10^{-6}	1.2×10^{-5}	1.5×10^{-5}	1.4×10^{-5}	2.0×10^{-5}	1.5×10^{-5}	1.2×10^{-5}	1.4×10^{-5}
R_2/Ω	36.81	22.1	20	27.23	18.107	15.97	29.46	33.259
$Q_2 - n$	0.7968	0.7272	0.6959	0.7725	0.9055	0.7074	0.7737	1
$Q_2 - Y_0/\Omega^{-1}\ s^n$	1.7×10^{-4}	6.0×10^{-4}	6.6×10^{-4}	8.7×10^{-4}	4.3×10^{-6}	7.0×10^{-4}	4.3×10^{-4}	3.2×10^{-6}
$Q_0 - n$	0.4452	0.4188	0.7881	0.8497	0.4319	0.4961	0.5503	0.5192
$Q_0 - Y_0/\Omega^{-1}\ s^n$	0.0206	0.0347	0.0638	0.0825	0.0352	0.033	0.0261	0.0177

with that of AC, while, there are no obvious pores for LFP. It is a slow process for the anionic groups (PF_6^{-1}) diffusing and absorbing onto all the available interface of AC/electrolyte. At the beginning of charge process, the resistance is large due to the polarization originated from the movement of anionic flux. With charge proceeding, the polarization resistance is almost constant and the capacitance from AC increases with more and more anionic groups absorb to the interface of AC/electrolyte. When the entire available interface of AC/electrolyte absorbs the anionic groups, AC could be regarded as an ideal capacitor and the capacitance reaches the maximum, the ultimate-capacitance. Therefore, with the proceeding of charge, the impedance spectra show a clearer and clearer capacitive property.[49,50] On the other hand, at the beginning of discharge process, AC desorbs the absorbed anionic groups immediately, hence displays an obvious capacitive discharge profile, as shown in Fig. 2a. During the diffusion process of the anionic groups, AC undergoes a similar process as the charge process.

All the results suggesting that the presence of AC significantly changed the charge–discharge process of the composite electrode compared with the pure LFP electrode.

The synergy between LFP and AC

In the following section, we attempt to provide an interpretation on the synergy between LFP and AC in the composite electrodes.

The XRD patterns of LFP and 5%LAC together with that of standard LFP (JCPDS card no. is 40-1499) are shown in Fig. S1.† All diffraction peaks seen from both the samples can be indexed to crystalline LFP with a space group of *Pnmb*. No obvious peaks corresponding to AC were found owing to its amorphous structure and low content.[26] Fig. S4† shows the morphology and microstructure of LFP sample, AC sample, LFP electrode, and 5%LAC electrode. Fig. S4a and S4b† show that LFP consisted of irregular-shaped particles with sizes ranging from 300 nm to 1 μm. Meanwhile, a particle agglomeration can also be observed. Fig. S4c† shows that AC exhibited a typical bulk feature with particle sizes ranging from 5 to 10 μm. The AC contained oxygen-containing groups as confirmed by the energy dispersive X-ray (EDX) data shown in Fig. 4d. Fig. S4e† shows that LFP electrode displays a quite uniform distribution of the particles with bigger LFP particles dispersed among the smaller AB conducting agent (AB shows a smaller particle size of about 30 nm). Fig. S4f† exhibits clearly lattice fringes indicating perfect crystallinity of LFP. The width (5.18 Å) of neighbouring lattice fringes corresponds to the (020) plane of LFP. Fig. S4g† shows that, in 5%LAC electrode, LFP and AB particles homogenously occupy the empty space available between large AC bulks. Fig. S4f† exhibits the closely contact between amorphous AC and LFP crystal. The width (2.14 Å) of neighbouring lattice fringes corresponds to the (112) plane of LFP.

Fig. 8 shows the schematic illustrations of LFP electrode (Fig. 8a) and LAC electrode (Fig. 8b). From the structural

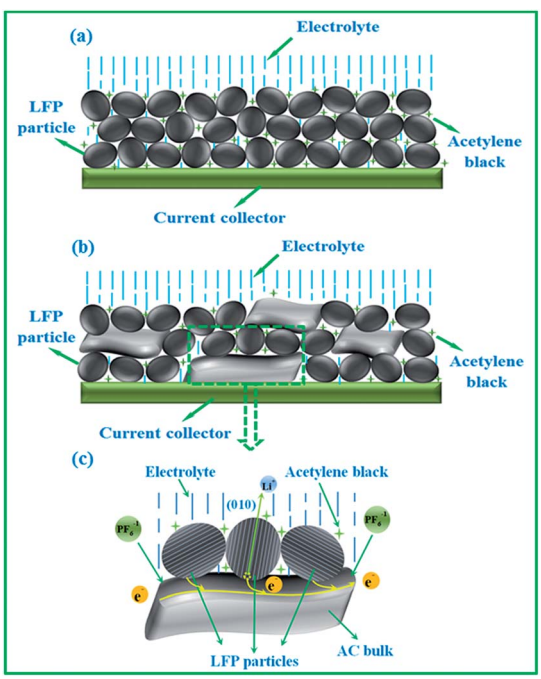

Fig. 8 The schematic illustrations of (a) LFP electrode, (b) LAC composite electrode and (c) partial enlarged details of LAC composite electrode at charge process.

perspective, after adding AC in composite electrodes, the agglomeration phenomenon of LFP particles can be decreased to some extent and the specific surface as well as the electronic conductivity of composite electrodes increased remarkably.[8,12] The Brunauer–Emmett–Teller (BET) surface areas of AC, LFP and 5%LAC estimated from the adsorption branches are 1241.6, 9.3 and 66.4 $m^2\ g^{-1}$ respectively. More information about BET can be seen from Fig. S2.† The electric conductivities of AC, LFP, 3%LAC, 5%LAC, 10%LAC and 15%LAC are 4.62×10^{-3} S cm^{-1}, 1.56×10^{-8} S cm^{-1}, 8.36×10^{-7} S cm^{-1}, 6.28×10^{-6} S cm^{-1}, 9.76×10^{-6} S cm^{-1} and 2.23×10^{-5} S cm^{-1} respectively, which indicates that a small addition of AC with large conductive surface area can effectively build the conductive web.[29,30] The BET surface areas and electric conductivities of AC, LFP and 5% LAC are compared in Table S1.† Moreover, during the charge and discharge processes, the interface reaction current density shared by AC is far less than that of LFP electrode at the same charge or discharge current rate, which ensures a superior rate performance of composite electrodes.

However, the addition of AC has no influence on the lithium ion diffusion coefficient – D_{Li} of LFP in composite electrodes. Under the condition of semi-infinite and infinite diffusion process, D_{Li} ($cm^2\ s^{-1}$) of LFP can be calculated by the following equation:[51]

$$D_{Li} = R^2T^2/2n^4F^4S^2\sigma^2C_{Li}{}^2 \quad (4)$$

where R is the gas constant (J K^{-1} mol^{-1}), T is the absolute temperature (K), S is the reaction surface area of the active component in the cathode (cm^2), n is the number of electrons per molecule during oxidization (here, $n = 1$), F is Faraday constant (C mol^{-1}), $C_{Li}{}^+$ is the concentration of lithium ion (about 1.7×10^{-2} mol cm^{-3}), σ is the Warburg factor ($\Omega\ s^{-1/2}$) related to Z'' (the imaginary part of cell impedance, ohm) and ω (the frequency, Hz) according to the following equation:[51]

$$-Z'' = \sigma\omega^{-1/2} \quad (5)$$

Fig. 9 shows $-Z''$ as a function of $\omega^{1/2}$ in the low frequency region with $x = 0.75$ in Li_xFePO_4 of charge process of both electrodes 5%LAC and LFP. The values of σ are 5.67 and 5.52 ($\Omega\ s^{-1/2}$) and the calculated lithium-ion diffusion coefficients of 5%LAC electrode and LFP electrode are 3.4×10^{-16} $cm^2\ s^{-1}$ and 2.9×10^{-16} $cm^2\ s^{-1}$, respectively. Fig. S5† compares D_{Li} of electrodes LFP and 5%LAC at different SOCs, in which the values of D_{Li} are calculated using the same method as $x = 0.75$. It can be seen that the D_{Li} of electrodes LFP and 5%LAC at the same SOC are similar, which indicate the addition of AC has no influence on D_{Li} of LFP in composite electrodes. Therefore, we believe that the electrochemical performances of LFP can be improved by interface modification of AC rather than changing the lithium ion diffusion coefficient, which in consistent with previous reports.[52]

As to the energy-storing perspective, there are two kinds of active materials in composite electrodes with two different energy-storing mechanisms – AC mainly stores energy in the double layer while LFP mainly store energy following a faradaic reaction. Potential as a function of time of AC electrode and LFP

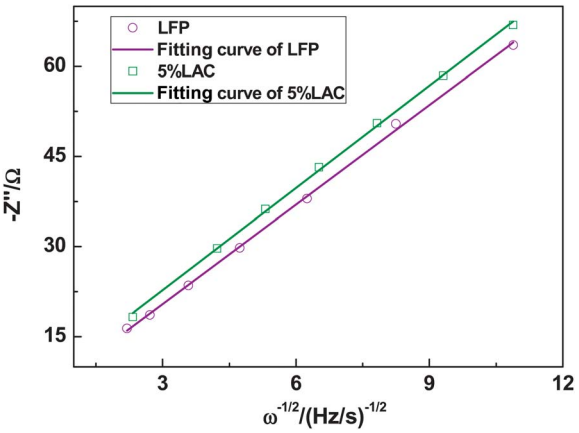

Fig. 9 $-Z''$ as a function of $\omega^{1/2}$ in the low frequency region with $x = 0.75$ in Li_xFePO_4 of charge process of both electrodes 5%LAC and LFP.

electrode at 1C–1D for both charge and discharge processes are shown in Fig. 10a and b, respectively. It can be seen that at the beginning of charge process, the potential of AC rises more rapidly than that of LFP, owing to much faster response for charging–discharging of AC in comparison with LFP.[53,54] When the potential of AC is higher than that of LFP, electrons will transfer from LFP to AC. From the microscopic view, as shown

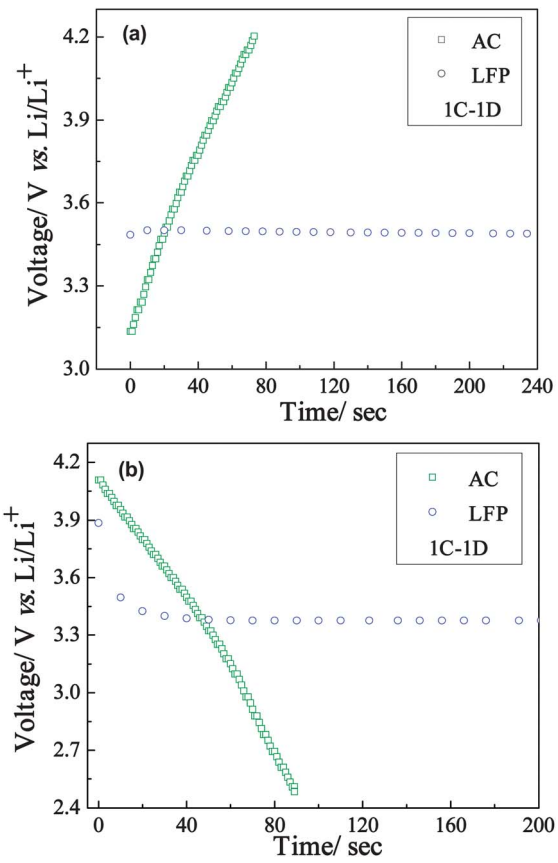

Fig. 10 Potential as a function of time of AC electrode and LFP electrode at 1C–1D for both charge (a) and discharge (b) processes.

in Fig. 8c – the partial enlarged details of LAC composite electrode, it could be recognized LFP is charged by AC. *Vice versa*, during the discharge process, the potential of AC decreases faster than that of LFP. When the potential of AC is lower than LFP, the electrons will transfer from the AC to LFP. In this way, a fast electron transferring channel could build between the two components and the synergy will emerge between the double layer charging process and faradaic reaction. In composite electrodes, AC component plays the role of "shock absorber" as it could quickly realizes capacity response buffering the impact to LFP under the condition of high-rate charging or discharging, which results in a preeminent rate performance and cycling property.

Conclusions

In this work, LAC composite electrodes with different mass ratios of LFP over AC are synthesized and the characteristics of the active materials and as-prepared electrodes are characterized by XRD, FESEM, HRTEM and BET analysis. After various kinds of electrochemical techniques testing, we delighted to find that the specific capacity, rate capability, fast-charge performance and cycling stability of the LAC composite electrodes are significantly improved due to the positive influence of AC. Especially, the composite electrode with 5 wt% AC exhibits the most enhanced performance in comparison with pure $LiFePO_4$ electrode, with a specific discharge capacity of 70 mA h g^{-1} at 20C while 100 mA h g^{-1} at 10 C without evident capacity-decay after 400 cycles. In order to further investigate the electrochemical characteristics of the composite electrode, electrochemical impedance spectroscopy (EIS) technique is employed to study the charge–discharge processes at different SOCs systematically for the first time.

Based on the experimental results, it suggests that between the two different active materials with different energy storage mechanisms – AC works as an electrochemical capacitor material (storing energy in electric double layer) while $LiFePO_4$ works as a Li-ion battery active material (storing energy utilizing a faradaic reaction) has a synergy between the two components, contributing to the observed excellent electrochemical performance.

Acknowledgements

The authors appreciate the support of National Natural Science Foundation of China (no. 50974045), the PhD Programs Foundation of Ministry of Education of China (no. 20092302110052), the Natural Science Foundation of Heilongjiang Province, China (no. B200918) and China Scholarship Council (no. 201206120186). Australian Research Council (ARC) is acknowledged for funding projects FT100100897 and DP130101870.

Notes and references

1 J. J. Wang and X. L. Sun, *Energy Environ. Sci.*, 2012, **5**, 5163.
2 D. Cericola, P. W. Ruch, R. Kötz, P. Novák and A. Wokaun, *Electrochem. Commun.*, 2010, **12**, 812.
3 M. Winter, J. O. Besenhard, M. E. Spahr and P. Novák, *Adv. Mater.*, 1998, **10**, 725.
4 M. R. Hill, G. J. Wilson, L. Bourgeois and A. G. Pandolfo, *Energy Environ. Sci.*, 2011, **4**, 965.
5 M. Winter and R. J. Brodd, *Chem. Rev.*, 2004, **104**, 4245.
6 J. Liu, T. E. Conry, X. Y. Song, M. Doeff and T. J. Richardson, *Energy Environ. Sci.*, 2011, **4**, 885.
7 J. T. Zhang and X. S. Zhao, *ChemSusChem*, 2012, **5**, 818.
8 D. Cericola, P. Novák, A. Wokaun and R. Kötz, *J. Power Sources*, 2011, **196**, 10305.
9 G. G. Amatucci, F. Badway, A. D. Pasquier and T. Zheng, *J. Electrochem. Soc.*, 2001, **148**, A930.
10 A. D. Pasquier, I. Plitz, S. Menocal and G. Amatucci, *J. Power Sources*, 2003, **115**, 171.
11 K. Karthikeyan, V. Aravindan, S. B. Lee, *et al.*, *J. Alloys Compd.*, 2010, **504**, 224.
12 D. Cericola, P. Novák, A. Wokaun and R. Kötz, *Electrochim. Acta*, 2011, **56**, 8403.
13 X. B. Hu, Z. H. Deng, J. H. Suo and Z. L. Pan, *J. Power Sources*, 2009, **187**, 635.
14 A. K. Padhi, K. S. Nanjundaswamy and J. B. Goodenough, *J. Electrochem. Soc.*, 1997, **144**, 1188.
15 M. S. Whittingham, *Chem. Rev.*, 2004, **104**, 4271.
16 M. Armand and J. M. Tarascon, *Nature*, 2008, **451**, 652.
17 Y. Wang and G. Z. Cao, *Adv. Mater.*, 2008, **20**, 2251.
18 Y. G. Wang, Y. R. Wang, E. J. Hosono, K. X. Wang and H. S. Zhou, *Angew. Chem., Int. Ed.*, 2008, **47**, 7461.
19 X. L. Wu, L. Y. Jiang, F. F. Gao, Y. G. Guo and L. J. Wan, *Adv. Mater.*, 2009, **21**, 2710.
20 F. Yu, J. J. Zhang, Y. F. Yang and G. Z. Song, *J. Mater. Chem.*, 2009, **19**, 9121.
21 C. Sun, S. Rajasekhara, J. B. Goodenough and F. Zhou, *J. Am. Chem. Soc.*, 2011, **133**, 2132.
22 Q. M. Wang, D. L. Wang and B. Wang, *Int. J. Electrochem. Sci.*, 2012, **7**, 8753.
23 Q. M. Wang, D. L. Wang and B. Wang, *Ionics*, 2013, **19**, 245.
24 B. Wang, D. L. Wang, Q. M. Wang, T. F. Liu, C. F. Guo and X. S. Zhao, *J. Mater. Chem. A*, 2009, **1**, 135.
25 A. G. Pandolfo and A. F. Hollenkamp, *J. Power Sources*, 2006, **157**, 11.
26 X. B. Hu, Y. J. Huai, Z. J. Lin, J. S. Suo and Z. H. Deng, *J. Electrochem. Soc.*, 2007, **154**, A1026.
27 X. B. Hu, Z. J. Lin, L. Liu, Y. J. Huai and Z. H. Deng, *J. Serb. Chem. Soc.*, 2010, **75**, 1259.
28 S. L. Chen, H. C. Hu, C. Q. Wang, G. L. Wang and J. L. Yin, *J. Renewable Sustainable Energy*, 2012, **4**, 033114.
29 N. Böckenfeld, T. Placke, M. Winter and A. Balducci, *Electrochim. Acta*, 2012, **76**, 130.
30 N. Böckenfeld, R.-S. Kühnel, S. Passerini, M. Winter and A. Balducci, *J. Power Sources*, 2011, **196**, 4136.
31 J. P. Schmidt, T. Chrobak, M. Ender, J. Illig, D. Klotz and E. Iver-Tiffée, *J. Power Sources*, 2011, **196**, 5342.
32 A. Krause, P. Kossyrev, M. Oljaca, S. Passerini, M. Winter and A. Balducci, *J. Power Sources*, 2011, **196**, 8836.
33 F. Pico, J. Ibanez, T. A. Centeno, C. Pecharroman, R. M. Rojas, J. M. Amarilla and J. M. Rojo, *Electrochim. Acta*, 2006, **51**, 4693.

34 C. Y. Wu, G. S. Cao, J. Xie and X. B. Zhao, *J. Phys. Chem. C*, 2011, **115**, 23090.
35 C. H. Chen, J. Liu and K. Amine, *J. Power Sources*, 2001, **96**, 321.
36 J. Y. Song, H. H. Lee, Y. Y. Wang and C. C. Wang, *J. Power Sources*, 2002, **111**, 255.
37 D. A. López, S. N. Simison and S. R. Sánchez, *Corros. Sci.*, 2005, **47**, 735.
38 Q. C. Zhuang, T. Wei, L. L. Du, Y. L. Cui, L. Fang and S. G. Sun, *J. Phys. Chem. C*, 2010, **114**, 8614.
39 N. Schweikert, H. Hahn and S. Indris, *Phys. Chem. Chem. Phys.*, 2011, **13**, 6234.
40 M. Takahashi, S. Tobishima, K. Takei and Y. J. Sakurai, *Solid State Ionics*, 2002, **148**, 283.
41 J. P. Schmidt, T. Chrobak, M. Ender, J. Illig, D. Klotz and E. Ivers-Tiffée, *J. Power Sources*, 2011, **196**, 5342.
42 J. Illig, M. Ender, T. Chrobak, J. P. Schmidt, D. Klotz and E. Ivers-Tiffée, *J. Electrochem. Soc.*, 2012, **159**, A952.
43 C. Arbizzani, M. Catellani, M. MaStragostino and C. Mingazzini, *Electrochim. Acta*, 1995, **40**, 1871.
44 D. Qu and H. Shi, *J. Power Sources*, 1998, **74**, 99.
45 L. Wang, J. S. Zhao, X. M. He, J. Gao, J. J. Li, C. R. Wan and C. Y. Jiang, *Int. J. Electrochem. Sci.*, 2012, **7**, 345.
46 J. S. Zhao, L. Wang, X. M. He, C. R. Wan and C. Y. Jiang, *Int. J. Electrochem. Sci.*, 2010, **5**, 478.
47 X. M. Liu, R. Zhang, L. Zhan, D. H. Long, W. M. Qiao, J. H. Yang and L. C. Ling, *New Carbon Mater.*, 2007, **22**, 153.
48 Q. Wang, J. L. Li, F. Gao, W. S. Li, K. Z. Wu and X. D. Wang, *New Carbon Mater.*, 2008, **23**, 275.
49 M. D. Stoller, S. J. Park, Y. W. Zhu, J. H. An and R. S. Ruoff, *Nano Lett.*, 2008, **8**, 3498.
50 C. Largeot, C. Portet, J. Chmiola, P. L. Taerna, Y. Gogotsi and P. Simon, *J. Am. Chem. Soc.*, 2008, **130**, 2730.
51 H. B. Shu, X. Y. Wang, Q. Wu, *et al.*, *J. Electrochem. Soc.*, 2011, **158**, A1448.
52 B. Kang and G. Ceder, *Nature*, 2009, **458**, 190.
53 A. Khaligh and Z. H. Li, *IEEE Trans. Veh. Technol.*, 2010, **59**, 2806.
54 A. Khaligh, A. M. Rahimi and Y. J. Lee, *IEEE Trans. Veh. Technol.*, 2007, **56**, 3709.